Journal of
Mechanics of
Materials and Structures

FRACTURE DEVELOPMENT ON A WEAK INTERFACE NEAR A WEDGE

Alexander N. Galybin, Robert V. Goldstein and Konstantin B. Ustinov

Volume 10, No. 3 May 2015

msp

JOURNAL OF MECHANICS OF MATERIALS AND STRUCTURES
Vol. 10, No. 3, 2015
dx.doi.org/10.2140/jomms.2015.10.265

FRACTURE DEVELOPMENT ON A WEAK INTERFACE NEAR A WEDGE

ALEXANDER N. GALYBIN, ROBERT V. GOLDSTEIN AND KONSTANTIN B. USTINOV

Formation of a fracture consisting in shear-opening delamination and Coulomb's frictional sliding zones along a weak interface in an elastic isotropic homogeneous plane subjected to wedging and external compression is studied. The shear-opening delamination is modelled by a mixed-mode crack; the frictional sliding zones are modelled by pure shear cracks. The interface is assumed to be much weaker than the material of the plane, so that only interface cracks are considered. The wedge is modelled by a pair of edge dislocations. Two particular cases have been considered: far-field and near-field asymptotics, corresponding to the cases of large and small ratios of the distance between the wedge and the interface and the distance between two dislocations modelling the wedge, respectively.

The possibility of formation of finite sliding zones ahead of the delamination on the weak interface is demonstrated. It is shown that, depending on the combination of external parameters (ratio of the dislocation burgers vector and elastic modulus, distance from the dislocation to the interface, magnitude of applied compression, cohesion and friction angle of the interface), two configurations of cracks may be observed: one mixed-mode crack, and three cracks — one central mixed mode crack and two external symmetrical shear cracks. The central part of the sliding zone is also open.

1. Introduction

Delamination occurring on a part of a weak interface ahead of an approaching fracture is explained by the presence of the tensile stress component parallel to the fracture; see [Cook et al. 1964]. This phenomenon is observed in various materials in lab experiments as well as in nature; e.g., dyke-sill transformations; see [Gudmundsson 2011]. It is widely accepted (see the references above) that the delamination can affect the crack propagation throughout the interface or serve as a barrier for crack arrest. Besides crack growth, there are other situations that may also lead to interface destruction, such as, for instance, wedging due to thermal expansion or rockmass fracturing near excavations. It should be understood that, in addition to tensile stresses, the interface is also subjected to shear stresses that can be high enough to affect the fracture processes developing on the interface. Experiments [Goldstein and Osipenko 2012; 2015] have shown that the appearance of sliding zones over the interface is capable of initiating secondary cracks perpendicular to the interface. Somewhat similar mechanisms are reported in [Zhou et al. 2010] for hydrofracture modelling.

There are numerical studies of fracture development on weak interfaces; e.g., [Cooke and Underwood 2001; Akulich and Zvyagin 2008]. These studies model both delamination and slip on the interface without employing any fracture characteristics (e.g., stress intensity factors or energy release rate) that control fracture, which is a serious drawback. Early work by Galybin [1997] takes into account fracture characteristics for the determination of the length of the sliding zones but do not consider delamination.

Keywords: mixed-mode interface crack, edge dislocation, delamination, sliding, singular integral equations.

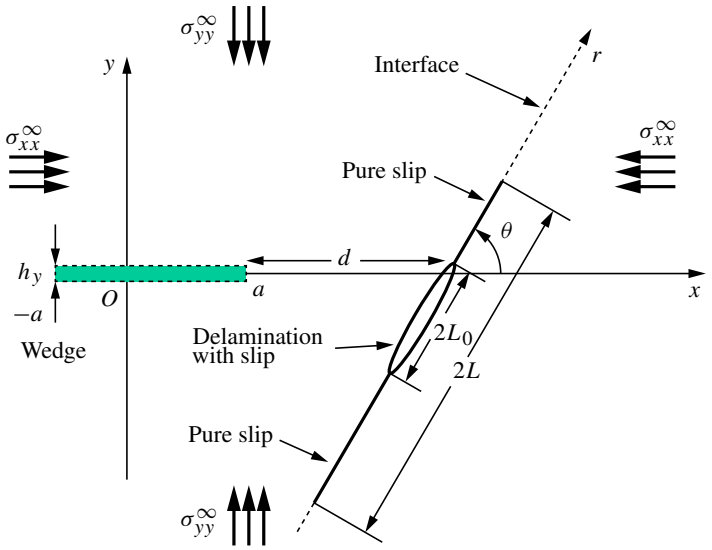

Figure 1. Geometry and loads.

Cracks at the interface of Coulomb's friction type between elastic and rigid bodies were considered in works by Bui and Oueslati [2004; 2005] and Bui [2006] with and without delamination. They obtained analytical solutions, with the emphasis on possible nonuniqueness arising from nonlinearity of the frictional contact crack problem and dependency of the solution on the (unspecified) loading history. The nonuniqueness and path dependence of the solution for problems involving Coulomb's friction contact was also emphasised in works of Dundurs and Comninou [1981; 1983] and Mendelsohn and Whang [1988].

In this study we model both delamination (as combined mode I-mode II cracks) and sliding zones (mode II cracks) caused by a wedge (modelled by edge dislocations) in a compressed elastic plane with a weak interface (which is considered as a plane of reduced strength). The sizes of opening and sliding zones are found from the solution. The back influence of the interface cracks on the dislocations is not taken into account, which allows one to apply the method suggested in [Galybin and Mukhamediev 2012; 2014] for estimation of the size of the delamination and the length of the pure sliding zones. The case with both opening and shear zones along the interface was studied before, for example by Gorbatikh et al. [2001]. Their work deals with the case when a part of the contour is traction-free under compressive normal loads at infinity, and the size of this traction-free zone is prescribed by the geometry of the problem. Such a formulation makes sense when a narrow cavity of certain special form is cut out from the plane.

The configuration shown in Figure 1 is studied. The ends of the delamination zone $(-L_0, L_0)$ are determined from the condition $K_{\mathrm{I}} = 0$, and the ends of the pure sliding zones $(-L, L)$ ("shear crack" in the figure) from the condition $K_{\mathrm{II}} = 0$, where K_{I} and K_{II} are the stress intensity factors for opening and transverse shear modes, respectively. Moreover, a more general case is considered, for which the shear zones appear also on two symmetric intervals outside the interval $(-L, L)$. For this case a system of three nonlinear equations will be examined.

2. Wedge in elastic plane

The complex potentials that characterise the stress field of an isotropic elastic plane with an edge dislocation of magnitude $h = h_x + ih_y$ whose core is placed at a point z_0 have the form [Muskhelishvili 1977]

$$\Phi(z) = \frac{H}{z - z_0}, \quad \Psi(z) = \frac{\bar{H}}{z - z_0} + \frac{\bar{z}_0 H}{(z - z_0)^2}, \tag{1}$$

where, for the condition of plane strain, one has

$$H = -\frac{iG(h_x + ih_y)}{\pi(1 + \kappa)}, \quad \kappa = 3 - 4\nu, \tag{2}$$

where G is the shear modulus of the plane and ν is Poisson's ratio. Note that the minus sign in (2) is due to the assumption that the cut is made to the left from the core, which can be directly checked by using the Kolosov–Muskhelishvili formulas for the displacements.

Let us assume that $z_0 = a$, $h_x = 0$ and $h_y = h > 0$; this also means that $H = \bar{H} > 0$, which results in the following expressions for the complex potentials:

$$\Phi_1(z) = \frac{H}{z - a}, \quad \Psi_1(z) = -z\Phi_1'(z) = \frac{zH}{(z - a)^2}. \tag{3}$$

Let us introduce the second dislocation, with the core at the point $z_0 = -a$ and with magnitude $h_x = 0$ and $h_y = -h > 0$ (thus, H in (3) should be replaced by $-H$); then the previous expressions for the complex potentials yield

$$\Phi_2(z) = \frac{-H}{z + a}, \quad \Psi_2(z) = -z\Phi_2'(z) = \frac{-zH}{(z + a)^2}. \tag{4}$$

The superposition of the stress fields (3) and (4) gives

$$\Phi_{\text{wedge}}(z) = \frac{S}{z^2 - a^2}, \quad \Psi_{\text{wedge}}(z) = -z\Phi_{\text{wedge}}'(z) = \frac{2z^2 S}{(z^2 - a^2)^2}, \quad S = 2aH. \tag{5}$$

The complex potentials in (5) give the solution for the wedge of finite length inserted into the elastic plane. Here S is a parameter that has dimension of force, and it is proportional to the area of the wedge penetrated into the plane. We further assume this value to be a constant.

By using the Kolosov–Muskhelishvili formulas one obtains the following expressions for the mean stresses $P = 0.5(\sigma_x + \sigma_y)$ and for the complex stress deviator function $D = 0.5(\sigma_y - \sigma_x) + i\sigma_{xy}$:

$$P(z, \bar{z}) = \Phi + \bar{\Phi} = \frac{S}{z^2 - a^2} + \frac{S}{\bar{z}^2 - a^2}, \quad D(z, \bar{z}) = \bar{z}\Phi' + \Psi = (\bar{z} - z)\Phi' = \frac{2z(z - \bar{z})S}{(z^2 - a^2)^2}. \tag{6}$$

The normal (σ_{nn}) and shear (σ_{nt}) stresses acting on an inclined plane (at an angle θ_0 to the x-axis) are given by

$$\sigma_n - i\sigma_t = P(z, \bar{z}) + e^{2i\theta_0} D(z, \bar{z}) = 2S\left[\operatorname{Re} \frac{1}{z^2 - a^2} + e^{2i\theta_0} \frac{z(z - \bar{z})}{(z^2 - a^2)^2}\right]. \tag{7}$$

Let us assume that a weak interface is located on a line (see Figure 1) specified by

$$z = a + w, \quad w = d + re^{i\theta}, \quad \theta = \text{const}, \tag{8}$$

where the value of $r = 0$ corresponds to the point of intersection of the interface with the continuation of the wedge line, the point $z = a + d$ in Figure 1.

Then the stresses on the interface can be presented in the form

$$\sigma_n - i\sigma_t = \frac{2S}{(a+d)^2}\left[\mathrm{Re}\,\frac{1}{(1+\rho e^{i\theta})^2-\delta^2} + \frac{2i\rho\sin\theta e^{2i\theta}(1+\rho e^{i\theta})}{((1+\rho e^{i\theta})^2-\delta^2)^2}\right], \quad \rho = \frac{r}{a+d}, \quad \delta = \frac{a}{a+d}. \tag{9}$$

Hereafter, σ_n and σ_t are the normal and shear components of stress along the interface.

We consider two configurations:

Configuration 1 (far field asymptotics). Assume that $a \ll |w|$ ($a \ll d$). Then the complex potentials in (5) become

$$\Phi_{\mathrm{wedge}}(z) = \frac{S}{z^2}, \quad \Psi_{\mathrm{wedge}}(z) = -z\Phi'_{\mathrm{wedge}}(z) = \frac{2S}{z^2}, \quad S = \mathrm{const}\,. \tag{10}$$

This asymptotic behavior coincides with the far field asymptotics for a mode I crack of length $2a$ and average opening S/G.

The stresses on the interface are found from (9) to be

$$\sigma_n - i\sigma_t = \frac{2S}{d^2}\left[\mathrm{Re}\,\frac{1}{(1+\rho e^{i\theta})^2} + \frac{2i\rho\sin\theta e^{2i\theta}}{(1+\rho e^{i\theta})^3}\right], \quad \rho = \frac{r}{d}. \tag{11}$$

The expression in brackets in (11) represents dimensionless stresses (normalised by $2S/d^2$) acting on the interface far from the wedge. They are shown in Figure 2 as functions of ρ for different interface inclinations.

Configuration 2 (near field asymptotics). Let us assume that $|w| \ll a$ ($d \ll a$). Then the stress functions in (6) take the form

$$P(w,\bar{w}) = \frac{S}{2a}\frac{w+\bar{w}}{w\bar{w}}, \quad D(w,\bar{w}) = \frac{S}{2a}\frac{w-\bar{w}}{w^2}. \tag{12}$$

It should be noted that these functions correspond to the case of a single dislocation with the core at the origin (they can also be found from (3) by assuming that $a = 0$, because $2aH = S$). The stresses on the interface are obtained from (12) in the form

$$\sigma_n - i\sigma_t = \frac{S}{ad}\left[\mathrm{Re}\,\frac{1}{1+\rho e^{i\theta}} + \frac{i\rho e^{2i\theta}\sin\theta}{(1+\rho e^{i\theta})^2}\right], \quad \rho = \frac{r}{d}. \tag{13}$$

The dimensionless (normalised by $S/(ad)$) stresses on the interface located close to the right end of the wedge are shown in Figure 3 for various interface inclinations as functions of ρ.

Comparing the stress profiles in Figures 2 and 3, one can notice that the stress distributions look qualitatively similar to each other. For the general configuration they differ only quantitatively from those depicted in Figures 2 and 3 for the full range of the parameters a, d and R. It should be noted that the dimensional magnitudes of the stresses near the wedge are much greater than their values far from the wedge. Thus, interface fracturing due to the stresses induced by the wedge is most likely to occur close to the wedge. Therefore, we further restrict our consideration to Configuration 2, which also allows one to reduce the number of parameters controlling the stress field.

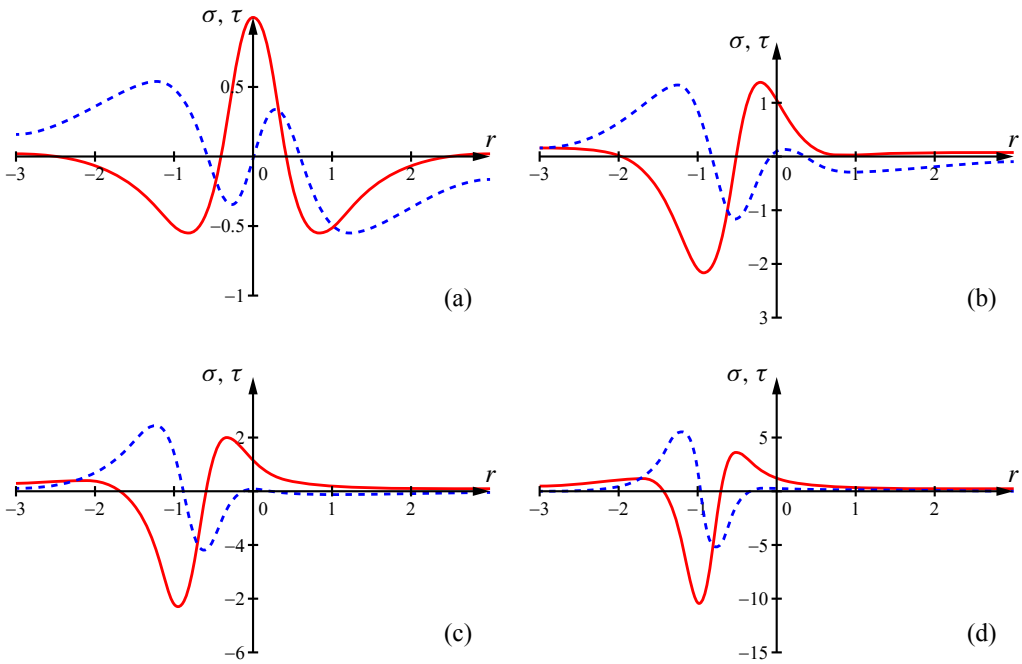

Figure 2. Profiles of dimensionless stresses caused by the wedge on the interface inclined at (a) $\theta = \pi/2$, (b) $\theta = \pi/3$, (c) $\theta = \pi/4$, (d) $\theta = \pi/6$ for Configuration 1 as functions of the parameter ρ; solid lines are normal stresses, dashed lines are shear stresses.

The total stresses should also reflect the remote loads, which create the following stresses on the interface:

$$\sigma_n^0 - i\sigma_t^0 = \frac{\sigma_{yy}^\infty + \sigma_{xx}^\infty}{2} + e^{2i\theta}\frac{\sigma_{yy}^\infty - \sigma_{xx}^\infty}{2} = \sigma_{yy}^\infty \cos^2\theta + \sigma_{xx}^\infty \sin^2\theta + i(\sigma_{yy}^\infty - \sigma_{xx}^\infty)\cos\theta\sin\theta. \quad (14)$$

It is evident from (14) that, for the case of compressive loads at infinity, the shear stresses on the interface can be of any sign depending on the difference of principal stresses at infinity, while the normal stress is always negative. The latter means that the external stress can compensate for the tensile normal stresses on the interface caused by the wedge. However, when the distance d is small, the stress magnitudes are unbounded, which indicates that the remote stresses cannot compensate for the stress concentration near the wedge, and hence a delamination zone should appear on the interface regardless of compression at infinity. The position of this zone depends on the interface inclination angle. As is evident from the profiles of normal stresses in Figure 3, for steep angles the delamination zone has to appear close to the point $z = a + d$, while for shallow angles the middle of this zone should be shifted to the left and down as shown in Figure 1. This delamination zone is also subjected to shear stresses that induce relative slip of the delamination surfaces. The direction of the slip is defined by the sign of the total shear stress, which can alternate. If the shear stresses due to remote loads are negative (vertical compression dominates) then the slip in the leftward direction should dominate (as the peak of the shear stresses caused by the wedge is also negative). In general, the slip zone can be longer than the delamination zone, and includes some

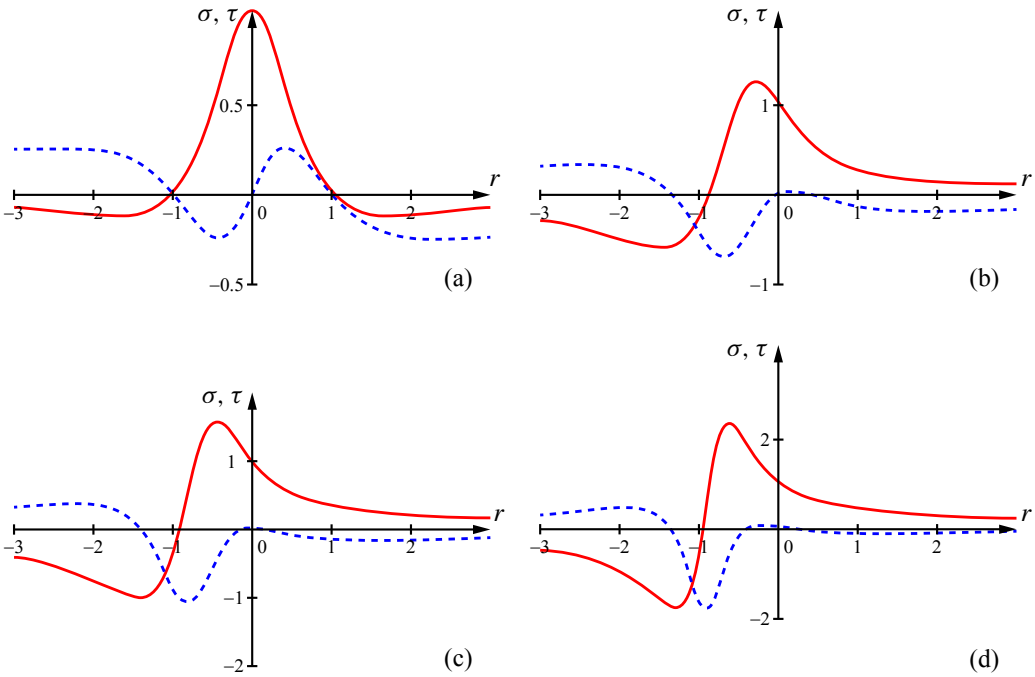

Figure 3. Profiles of dimensionless stresses caused by the wedge on the interface inclined at (a) $\theta = \pi/2$, (b) $\theta = \pi/3$, (c) $\theta = \pi/4$, (d) $\theta = \pi/6$ for Configuration 2 as functions of the parameter ρ; solid lines are normal stresses, dashed lines are shear stresses.

parts with pure slip, as shown in Figure 1. Therefore one arrives at the problem, in which the opening zone is placed within the shear zone.

We further model the delamination zone as a combined mode I–mode II crack (contour Γ_0) and the pure slip zones as mode II cracks (contour Γ_1). In the latter case there is no crack opening, which means that the normal displacement u_n is continuous across the crack contour Γ_1. For simplicity we assume that the slip is subjected to the Mohr–Coulomb criteria. The boundary conditions of the problem can be presented in terms of total stresses as follows:

$$\begin{gathered} \sigma_n - i\sigma_t = 0 \quad \text{on } \Gamma_0, \\ |\sigma_t| = C - \sigma_n \tan\phi, \quad \sigma_n < 0, \quad u_n^+ = u_n^- \quad \text{on } \Gamma_1, \\ \sigma_{ij} \to \sigma_{ij}^\infty \quad \text{at infinity.} \end{gathered} \tag{15}$$

Here C is cohesion and ϕ is the friction angle along the weak interface; plus and minus stand for the upper and lower surfaces of the crack, respectively.

For simplicity we will further study the symmetric case of the perpendicular interface $\theta = \pi/2$; in this case the centre of the crack is placed at the point $z = d + i0$ and the contours are represented by the symmetric intervals $\Gamma_0 = (-L_0, L_0)$ and $\Gamma_1 = (-L, -L_0) \cup (L_0, L)$ of the range of the dimensionless parameter ρ. The total contour is further denoted as $\Gamma = \Gamma_0 \cup \Gamma_1 = (-L, L)$.

By introducing the dimensionless parameter

$$\tilde{H} = \frac{1}{\pi(1+\kappa)} \frac{G}{|\sigma_{xx}^{\infty}|} \frac{h_y}{d}, \tag{16}$$

one can present the dimensionless stresses (normalised by σ_{xx}^{∞}) on the interface as

$$\tilde{\sigma}_{xx}(\rho) = 2\tilde{H} \frac{1-\rho^2}{(1+\rho^2)^2}, \quad \tilde{\sigma}_{xy}(\rho) = 2\tilde{H} \frac{\rho(1-\rho^2)}{(1+\rho^2)^2}, \quad -\infty < \rho < +\infty. \tag{17}$$

Later on, the tilde sign over the dimensionless stresses and parameters is removed. The remote vertical compression does not play any role in symmetric arrangement, therefore $\sigma_{yy}^{\infty} = 0$.

It follows from (17) that the normal stresses due to the wedge are tensile on the interval $(-1, 1)$, with the maximum at $\rho = 0$, while the shear stresses change sign three times when crossing the points corresponding the values of the parameter $\rho = -1, 0, 1$; they have extrema of the same magnitudes at the points specified by the values $\rho = \pm\sqrt{2} \pm 1$. The profiles of (17) are shown in Figure 3a for $H = 1$. As mentioned, the maximum normal stresses on the interface are unbounded when d tends to zero. In the meantime, the size of the zone with tensile stresses also tends to zero when d tends to zero.

3. Singular integral equations for the cracks on the interface

Since the interface is subjected to tension and shear, it is possible that a combined open-shear crack appears in the central part and pure shear cracks at the periphery. These cracks can be considered separately because the normal opening does not induce shear stresses on the interface and the jump of the tangential displacement does not cause normal stresses.

The boundary conditions for the determination of the dimensionless normal stresses caused by crack opening, $\sigma_{xx}^{\text{crack}}$, on the interval $(-L_0, L_0)$ have the form

$$\sigma_{xx}^{\text{crack}}(y) - 1 + 2H \frac{1-y^2}{(1+y^2)^2} = 0, \quad |y| < L_0. \tag{18}$$

The second boundary condition in (15) for the determination of the dimensionless shear stresses caused by the crack opening, $\sigma_{xy}^{\text{crack}}$, on the interval $(-L, L)$ can be expressed in the piecewise form

$$\begin{aligned} &\sigma_{xy}^{\text{crack}}(y) + 2H \frac{y(1-y^2)}{(1+y^2)^2} = 0, \quad |y| < L_0, \\ &\left|\sigma_{xy}^{\text{crack}}(y) + 2H \frac{y(1-y^2)}{(1+y^2)^2}\right| = C - k\sigma_{xx}^{\text{total}}(y), \quad \sigma_{xx}^{\text{total}}(y) < 0, \quad |y| > L_0, \quad y \in \Gamma, \end{aligned} \tag{19}$$

where $k = \tan\phi$ is the friction coefficient and we have introduced the notation

$$\sigma_{xx}^{\text{total}}(y) = \sigma_{xx}^{\text{crack}}(y) - 1 + 2H \frac{1-y^2}{(1+y^2)^2}, \quad |y| > L_0. \tag{20}$$

A singular integral equation (SIE) for the problem in (18) has the form

$$\frac{1}{\pi} \int_{-L_0}^{L_0} \frac{u(t)}{t-y}\, dt = 1 - 2H \frac{1-y^2}{(1+y^2)^2}, \quad |y| < L_0. \tag{21}$$

Here $u(t)$ is a sought function proportional to the density of the normal displacement discontinuity on $(-L_0, L_0)$ that satisfies the condition of single-valuedness of the normal displacements

$$\int_{-L_0}^{L_0} u(t)\,dt = 0. \tag{22}$$

When deriving the SIE for the boundary value problem (19), one has to remove the absolute value sign in the left-hand side of the second equation in (19). This can be done by examining the directions of the total shear stresses. The shear stresses caused by the shear crack should have the opposite signs as those caused by the wedge in order to compensate for the excess in the left-hand side of the second formula in (19). Thus, the absolute value sign can be removed by introducing the step-like function

$$\chi(y) = \begin{cases} 0 & |y| < L_0, \\ \operatorname{sgn}[y(1-y^2)] & |y| > L_0. \end{cases} \tag{23}$$

As the result, the SIE for the problem specified by (19) takes the form

$$\frac{1}{\pi}\int_\Gamma \frac{v(t)}{t-y}\,dt = -2H\frac{y(1-y^2)}{(1+y^2)^2} + \chi(y)(C - k\sigma_{xx}^{\text{total}}(y)), \quad y \in \Gamma. \tag{24}$$

Here $v(t)$ is a sought function proportional to the density of the tangential displacement discontinuity on $(-L, L)$ that satisfies the condition of single-valuedness of the tangential displacements. The form of this condition depends on the number of pure slip zones of the entire contour. It is obvious that, due to the lack of friction on the central part, on the interval $(-L_0, L_0)$ the shear crack in the centre always has length greater than the length of the open zone. We further assume that the slip is on $(-L, L)$ and $L_0 < L$.

If the resistance to shear stresses is small, then the slip can also grow outside $(-L, L)$, where the intensity of the shear stresses is the same as in the middle, but they decay slowly (see Figure 3a). Let us further assume that the slip develops on the intervals $A < |y| < B$, such that the inequalities

$$0 < L_0 < L \le A \le B \tag{25}$$

hold and the entire contour Γ is given by

$$\Gamma = (-B, -A) \cup (-L, L) \cup (A, B). \tag{26}$$

Then the conditions of single-valuedness for the SIE (24) take the form

$$\int_{-B}^{-A} v(t)\,dt = 0, \quad \int_{-L}^{L} v(t)\,dt = 0, \quad \int_{A}^{B} v(t)\,dt = 0. \tag{27}$$

Note that if $A = B$ then it is necessary to satisfy the second condition in (27) only.

The mode I–mode II crack length can be estimated from a criterion of crack growth, in particular by knowing fracture toughness of the interface material, which requires calculation of the stress intensity factors $(K_{\text{I}}, K_{\text{II}})$, respectively, at the ends of all cracks. For the estimation of the maximum L_0 one can use the condition $K_{\text{I}} = 0$, otherwise the Mohr–Coulomb friction condition cannot be satisfied in the vicinity of the mode I crack end due to unbounded tensile normal stresses, which violates the inequality $\sigma_{xx}^{\text{total}}(y) < 0$ in the second condition in (19).

For the determination of the ends of the slip zones it is also reasonable to use the condition $K_{\mathrm{II}} = 0$, which allows one to determine the maximum possible lengths of all slip zones. As the stress intensity factors (SIFs) can be determined from the asymptotics of the sought function at the crack ends, one can employ the following conditions that address $K_{\mathrm{I}} = 0$ and $K_{\mathrm{II}} = 0$:

$$U(L_0) = 0, \quad V(L) = 0, \quad V(A) = 0, \quad V(B) = 0, \tag{28}$$

where

$$U(t) = u(t)\sqrt{L_0^2 - t^2}, \quad V(t) = v(t)\sqrt{(L^2 - t^2)(t^2 - B^2)(t^2 - A^2)}. \tag{29}$$

In the next section we find analytical expressions for the SIFs in both problems (21)–(22) and (24), (27).

4. Solution for the delamination zone

The solution of the SIE (21) unbounded at the ends and satisfying (22) is given by the formula (see for example [Muskhelishvili 1977])

$$u(t) = \frac{-1}{\pi\sqrt{L_0^2 - t^2}} \int_{-L_0}^{L_0} \frac{\sqrt{L_0^2 - x^2}}{x - t} \left(1 - 2H \frac{1 - x^2}{(1 + x^2)^2}\right) dx, \quad |t| < L_0. \tag{30}$$

The integral in the right-hand side of (30) can be evaluated analytically; the solution assumes the form

$$u(t) = \frac{t}{\sqrt{L_0^2 - t^2}} \left(1 + \frac{2H}{\sqrt{L_0^2 + 1}} \frac{t^2 - 2L_0^2 - 1}{(t^2 + 1)^2}\right). \tag{31}$$

The mode I SIF obtained from (31) has the form

$$\frac{K_{\mathrm{I}}}{\sigma_{xx}^{\infty}\sqrt{\pi L_0}} = 1 - 2H(L_0^2 + 1)^{-3/2}. \tag{32}$$

The length of the crack is determined from the condition $K_{\mathrm{I}} = 0$. This leads to the following relationships between the half-length L_0 and the parameter H:

$$2H = (L_0^2 + 1)^{3/2}, \quad L_0 = \sqrt{(2H)^{2/3} - 1}. \tag{33}$$

One of these parameters can be considered as independent; let it be L_0 from now on.

Then the solution bounded at both ends is given by the formula

$$u(t) = -t \frac{t^2 + 2L_0^2 + 3}{(t^2 + 1)^2} \sqrt{L_0^2 - t^2}. \tag{34}$$

Note that this solution exists for $2H > 1$, which holds if

$$\frac{1}{2\pi(1 - \nu)} \frac{G}{|\sigma_x^{\infty}|} > \frac{d}{h_y}. \tag{35}$$

It is evident from (35) that the solution does not exist only if the distance between the wedge and the interface is essentially greater than the wedge magnitude, i.e., if the shear modulus is greater than the remote compression.

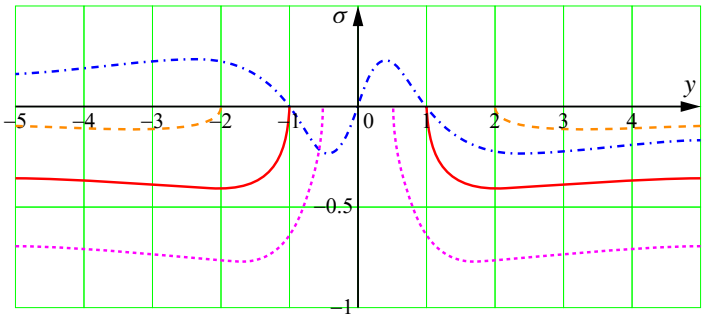

Figure 4. The stresses on the interface after delamination for $L_0 = 0.5, 1, 2$; dots are normal stress for $L_0 = 0.5$, solid line is normal stress for $L_0 = 1$, dashed line is normal stress for $L_0 = 2$, dash-dotted line is shear stress.

The crack growth is stable if $dK_I/dL_0 < 0$ and unstable if $dK_I/dL_0 > 0$. This derivative is always positive, because

$$\frac{dK_I}{dL_0} = \sigma_x^\infty \frac{d}{dL_0}\Big[\big(1 - 2H(L_0^2+1)^{-3/2}\big)\sqrt{\pi L_0}\Big] = 3\sigma_x^\infty \sqrt{\frac{\pi}{L_0}}\frac{L_0^2}{L_0^2+1} > 0. \tag{36}$$

This indicates that the growth is unstable.

The normal stresses on the interface caused by the mode I crack are found from the solution (34) by means of the integral

$$\sigma_{xx}^{\text{crack}}(y) = \frac{1}{\pi}\int_{-L_0}^{L_0} \frac{u(t)}{t-y}\,dt = \frac{-1}{\pi}\int_{-L_0}^{L_0} \frac{t}{t-y}\frac{t^2+2L_0^2+3}{(t^2+1)^2}\sqrt{L_0^2-t^2}\,dt. \tag{37}$$

Evaluation of the integral in the right-hand side of (37) yields

$$\sigma_{xx}^{\text{crack}}(y) = \frac{-1}{(1+y^2)^2}\Big[(1-(2L_0^2+1)y^2)\big(\sqrt{L_0^2+1}-1\big) + L_0^2\sqrt{L_0^2+1}(1+y^2) + (2L_0^2+3+y^2)\big(\sqrt{1-L_0^2/y^2}-1\big)\Big], \quad |y| > L_0. \tag{38}$$

The total stresses on the interfaces are found by substitution of (38) into (20) followed by simplifications:

$$\sigma_{xx}^{\text{total}}(y) = \frac{-y^2(y^2+2L_0^2+3)}{(1+y^2)^2}\sqrt{1-L_0^2/y^2}, \quad |y| > L_0. \tag{39}$$

Figure 4 shows the profiles of the dimensionless (divided by $2H$) shear (dash-dotted curve) and normal stresses after appearance of the delamination zone for $L_0 = 0.5, 1, 2$.

The normal stress attains its minimum at the point

$$y_{\min} = \sqrt{\frac{3L_0^4+5L_0^2+3+\sqrt{9L_0^4+6L_0^2+9}(L_0^2+1)}{3L_0^2+2}}. \tag{40}$$

The minimal values of the normal stresses, $\sigma_{\min}$, are shown in Figure 5 as a function of the half-length of the delamination zone, L_0. Note that $y_{\min} = \sqrt{3}$ at $L_0 = 0$, hence $\min \sigma_{xx}^{\text{total}} = -\frac{9}{8}$.

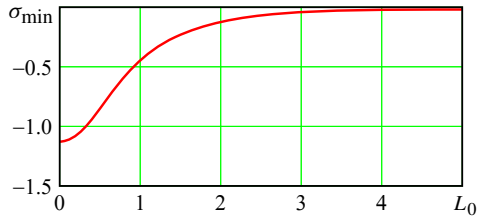

Figure 5. Minimum of normal stresses on the interface as a function of the half-length of the delamination L_0.

5. Solution for the slip zones

Let us introduce the function

$$F(y) = |\sigma_{xy}(y)| + k\sigma_{xx}^{\text{total}}(y) - C, \tag{41}$$

where $\sigma_{xy}(y) = -(L_0^2+1)^{3/2} y(1-y^2)(1+y^2)^{-2}$ is the dimensionless shear stress on the interface caused by the wedge with the delamination zone of the length determined with the use of (33).

The function $F(y)$ in (41) is actually the right-hand side of the SIE in (24). It should be positive ($F(y) > 0$) at least at one point in order for slip zones to appear over the interface. Three situations are shown in Figure 6 ($L_0 = 0.5, 1, 2$) to illustrate possible profiles of the function $F(y)$ for the strength parameters $k = \tan 15^\circ$ and $C = 0$.

As is evident from Figure 6, up to three sliding zones can be formed. For instance, at $L_0 = 0.5$ (dotted line), $F(y) < 0$ outside the central part, i.e., resistance to slip at the periphery is higher than the shear stress, thus one can expect the appearance of a single shear zone. At $L_0 = 1$ (solid line), two symmetric intervals exist where $F(y) > 0$, which indicates a possibility of three nonconnecting shear zones. When $L_0 = 2$ (dashed line), $F(y) > 0$, which corresponds to the case in which three pure shear cracks may coalesce into one (the slip directions could be different in different parts of this zone).

Let us consider the most typical cases.

It is seen from the figures above that the slip resistance depends on the half-length L_0 essentially. Thus, at $L_0 > 2$ one observes that $\min |\sigma_{xx}^{\text{total}}| < 0.12$, which, taking into account the friction coefficient

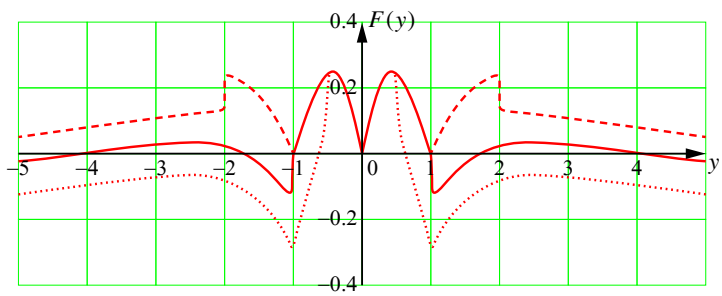

Figure 6. The function in (41) for the cases $L_0 = 0.5, 1, 2$ at $k = \tan 15^\circ$ and $C = 0.1$; dashed line corresponds to $L_0 = 2$, solid line corresponds to $L_0 = 1$, dotted line corresponds to $L_0 = 0.5$.

in the Mohr–Coulomb criterion, makes the term $k\sigma_{xx}^{\text{total}}$ insignificant as compared to the shear stresses, which vary within the range $0.18 < |\sigma_{xy}| < 0.25$ for $2 < y < 5$. If the remote compression is greater than cohesion then the term C in the SIE (24) is also small. Then the slip zones are mostly defined by the magnitudes of the shear stresses caused by the wedge; hence, the second term in (24) can be neglected. This means that the slip occurs over the interval $(-L, L)$, $L > L_0 > 2$, and $L = B$; see (25)–(26).

The mode II SIF at the right end of the slip zone can be found analytically as follows:

$$\frac{K_{\text{II}}}{|\sigma_x^\infty|\sqrt{\pi L}} = 2H\int_{-L}^{L}\sqrt{\frac{L+y}{L-y}}\,\frac{y(1-y^2)}{(1+y^2)^2}\,dy = -2H\pi\left(1-\frac{2L^2+1}{(L^2+1)^{3/2}}\right). \tag{42}$$

The right-hand side of (42) is zero at

$$L^* = \sqrt{\tfrac{1}{2}(1+\sqrt{5})} \approx 1.272,$$

which indicates that for the range $L > 2$ one has $K_{\text{II}} < 0$, i.e., the theoretical length of the sliding zone obtained by the condition $K_{\text{II}} = 0$ is infinite. In practice it can essentially exceed the length of the delamination zone provided that the latter is greater than the distance from the wedge to the interface.

One should note that the value $L^* = 1.272$ is the maximum possible half-length of the central mode II crack in the absence of friction and cohesion. In principle, it is possible that $L^* = L_0 = 1.272$ and simultaneously that $K_{\text{I}} = K_{\text{II}} = 0$, which is true if $H = 2.118$.

Let us analyse another limiting case, when the shear resistance on $A < |y| < B$ is greater than the shear stresses. Then the slip can occur only in the middle part $(-L, L)$. Moreover, on the interval $(-L_0, L_0)$, shear resistance is absent due to delamination. The dimensionless mode II SIF at the right end in this case is found by substituting (24) into the integral in (42):

$$\tilde{K}_{\text{II}} = \frac{K_{\text{II}}}{|\sigma_x^\infty|\sqrt{\pi L}} = 2H\int_{-L}^{L}\sqrt{\frac{L+y}{L-y}}\,\frac{y(1-y^2)}{(1+y^2)^2}\,dy - \int_{-L}^{L}\sqrt{\frac{L+y}{L-y}}\,\chi(y)(C-k\sigma_{xx}^{\text{total}}(y))\,dy. \tag{43}$$

Since the function $\chi(y)$ is odd (see (23)) and the term in the brackets is even, one can present the second integral in (43) in the form

$$\int_{-L}^{L}\sqrt{\frac{L+y}{L-y}}\,\chi(y)(C-k\sigma_{xx}^{\text{total}}(y))\,dy = 2\int_{L_0}^{L}\frac{y(C-k\sigma_{xx}^{\text{total}}(y))}{\sqrt{L^2-y^2}}\,dy. \tag{44}$$

The single shear crack can propagate inside different zones; for example, for $L_0 = 0.5$ in Figure 6 the slip can begin within the interval $(-1, 1)$, where the shear stress changes its direction at the origin. However, it is also possible that the slip could take place over the large zone including the interval $(-1, 1)$, as is shown, for example, for the case $L_0 = 1.5$, $k = \tan 15°$, $C = 0.2$ in Figure 7. In this case the slip directions will be different on opposite sides of the points $y = -1, +1$.

Therefore, the following three scenarios are possible:

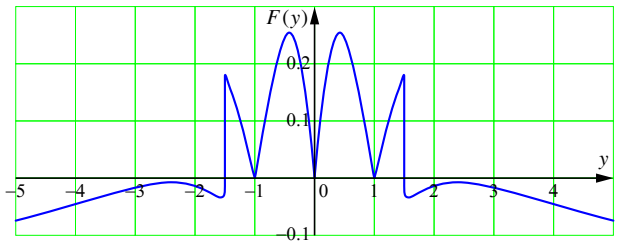

Figure 7. The function (41) for $L_0 = 1.5$ at $k = \tan 15^\circ$ and $C = 0.2$.

(1) If $L_0 > 1$, then $\chi(y) = -1$ and (44) takes the form

$$\int_{-L}^{L} \sqrt{\frac{L+y}{L-y}}\chi(y)(C - k\sigma_{xx}^{\text{total}}(y))\,dy = -\int_{L_0}^{L} \frac{2y(C - k\sigma_{xx}^{\text{total}}(y))}{\sqrt{L^2 - y^2}}\,dy$$
$$= -2C\sqrt{L^2 - L_0^2} + kG_1(L_0, L), \tag{45}$$

where

$$G_1(L_0, L) = \frac{2}{(1 + L_0^2)^{3/2}} \int_{L_0}^{L} \frac{\sqrt{y^2 - L_0^2}}{\sqrt{L^2 - y^2}} \frac{y^2(y^2 + 2L_0^2 + 3)}{(y^2 + 1)^2}\,dy. \tag{46}$$

In this case the final expression for K_{II} can be presented in the form

$$\tilde{K}_{\text{II}} = -\pi(L_0^2 + 1)^{3/2}\left(1 - \frac{2L^2 + 1}{(L^2 + 1)^{3/2}}\right) + 2C\sqrt{L^2 - L_0^2} + kG_1(L_0, L). \tag{47}$$

(2) If $L_0 < L < 1$, then $\chi(y) = 1$ and (44) has a form similar to (45) but with the opposite sign, hence the expression for K_{II} takes the form

$$\tilde{K}_{\text{II}} = -\pi(L_0^2 + 1)^{3/2}\left(1 - \frac{2L^2 + 1}{(L^2 + 1)^{3/2}}\right) - 2C\sqrt{L^2 - L_0^2} - kG_1(L_0, L). \tag{48}$$

(3) If $L_0 < 1$, then $\chi(y)$ can alter its sign, and if $L > 1$, then it is necessary to consider two integrals, hence (44) takes the form

$$\int_{-L}^{L} \sqrt{\frac{L+y}{L-y}}\chi(y)(C - k\sigma_{xx}^{\text{total}}(y))\,dy$$
$$= \int_{L_0}^{1} \frac{2y(C - k\sigma_{xx}^{\text{total}}(y))}{\sqrt{L^2 - y^2}}\,dy - \int_{1}^{L} \frac{2y(C - k\sigma_{xx}^{\text{total}}(y))}{\sqrt{L^2 - y^2}}\,dy$$
$$= \int_{L_0}^{L} \frac{2y(C - k\sigma_{xx}^{\text{total}}(y))}{\sqrt{L^2 - y^2}}\,dy - 2\int_{1}^{L} \frac{2y(C - k\sigma_{xx}^{\text{total}}(y))}{\sqrt{L^2 - y^2}}\,dy$$
$$= 2C\left(\sqrt{L^2 - L_0^2} - 2\sqrt{L^2 - 1}\right) - k(G_1(L_0, L) - 2G_2(L_0, L)), \tag{49}$$

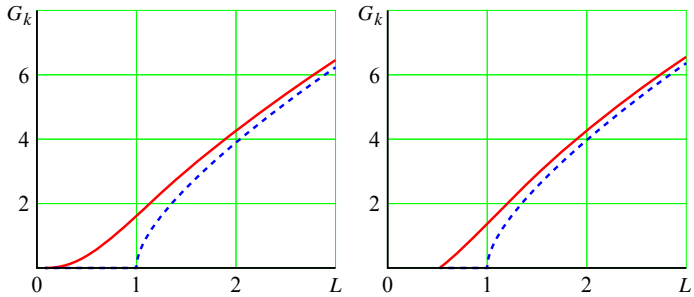

Figure 8. The integrals $G_k(L_0, L)$ as functions of L (solid curve for G_1, dashed curve for G_2). Left: $L_0 = 0.1$. Right: $L_0 = 0.5$.

where

$$G_2(L_0, L) = \frac{2}{(1+L_0^2)^{3/2}} \int_{L_0}^{1} \frac{\sqrt{y^2 - L_0^2}}{\sqrt{L^2 - y^2}} \frac{y^2(y^2 + 2L_0^2 + 3)}{(y^2+1)^2}\, dy. \tag{50}$$

If $L_0 < 1$ and $L > 1$, then the final expression for K_{II} is

$$\tilde{K}_{\mathrm{II}} = -\pi(L_0^2+1)^{3/2}\left(1 - \frac{2L^2+1}{(L^2+1)^{3/2}}\right) - 2C\left(\sqrt{L^2 - L_0^2} - 2\sqrt{L^2-1}\right) - k(G_1(L_0, L) - 2G_2(L_0, L)). \tag{51}$$

The integrals $G_k(L_0, L)$, $k = 1, 2$, can be expressed as elliptical integrals or computed numerically. Their typical behaviour is illustrated in Figure 8.

The dependence of K_{II} on L is shown in Figures 9–11 for the various strength parameters (cohesion and friction coefficient) at $L_0 = 0.5$.

The nearest root of the equation that comes from the condition $K_{\mathrm{II}} = 0$ should be selected for the determination of the mode II crack length. It is evident from the figure that for $L_0 = 0.5$ the sliding zone length is usually less than one, apart from the case when the shear resistance is absent (solid curve in Figure 9, left) or cohesion is negligible for low friction angles (solid curve in Figure 9, right). In the latter case the length of the zone is greater than $L^* = 1.252$.

The half-length of the sliding zones determined by the condition $K_{\mathrm{II}} = 0$ are shown in Figure 11 for various lengths of the delamination zones, for $k = \tan 30°$.

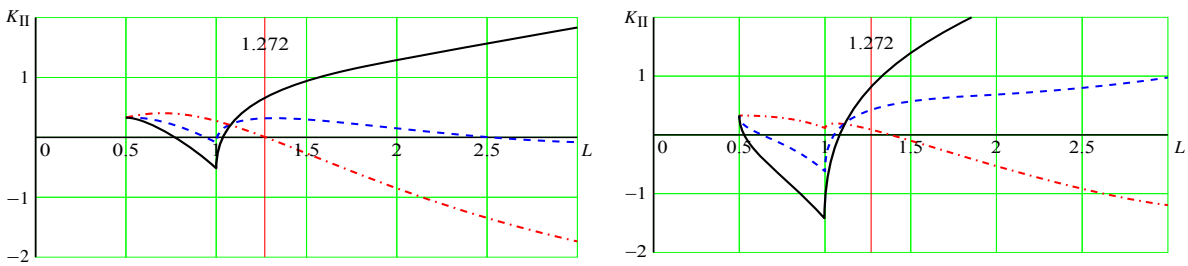

Figure 9. Dependence of dimensionless K_{II} on L for various values of the friction angle (left) and the cohesion (right), for $L_0 = 0.5$ and $C = 0$; dash-dotted line corresponds to $\rho = 0°$, dashed line to $\rho = 15°$, solid line to $\rho = 30°$.

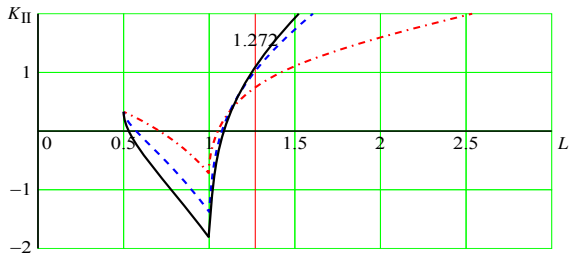

Figure 10. Dependence of dimensionless K_{II} on L for various combinations of the friction angles and cohesion for $L_0 = 0.5$; dash-dotted line corresponds to $\rho = 0°$, dashed line corresponds to $\rho = 15°$, solid line corresponds to $\rho = 30°$.

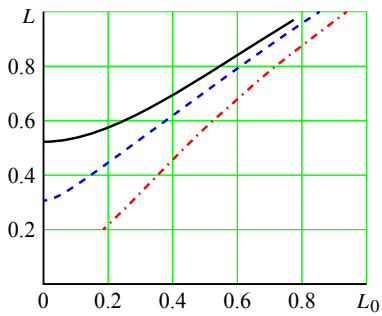

Figure 11. The half-length of the sliding zone L as a function of the half-length of the delamination zone L_0 for various cohesions at $k = \tan 30°$; dash-dotted line corresponds to $C = 0.5$, dashed line corresponds to $C = 0.1$, solid line corresponds to $C = 0.5$.

6. Three sliding zones

In order to find the length of the sliding zones one can employ the solution presented in [Gakhov 1966] for the inversion of the Cauchy integrals on m open contours:

$$\frac{1}{\pi}\int_\Gamma \frac{\varphi(t)}{t-\tau}\,dt = f(\tau). \tag{52}$$

The solution bounded at all ends has the form

$$\varphi(t) = -R(t)\frac{1}{\pi}\int_\Gamma \frac{f(\tau)}{R(\tau)}\frac{d\tau}{\tau - t}. \tag{53}$$

This is possible if the following conditions are satisfied:

$$\int_\Gamma \frac{f(\tau)}{R(\tau)}\tau^{j-1}\,d\tau = 0, \quad j = 1, \ldots, m, \tag{54}$$

where $R(z)$ is a complex-valued function defined by

$$R(z) = \prod_{k=1}^{m}\sqrt{(z-a_k)(z-b_k)}. \tag{55}$$

In the case considered it is possible that three symmetric slip zones can appear on a straight line; therefore formula (55) takes the form

$$R(t) = \sqrt{(t^2 - A^2)(t^2 - B^2)(L^2 - t^2)}, \quad \operatorname{Im} t = 0. \tag{56}$$

The right-hand side of (24) should be used as the function $f(t)$ in (54). The conditions in (54) are automatically satisfied for $j = 1, 3$ due to the odd right-hand side in (33). The rest take the form

$$\int_0^L \frac{h(y)}{R(y)} y\, dy + \int_A^B \frac{h(y)}{R(y)} y\, dy = 0, \tag{57}$$

where we denote

$$h(y) = \tfrac{1}{2}(f(y) - f(-y)) = -(L_0^2 + 1)^{3/2} \frac{y(1 - y^2)}{(1 + y^2)^2} + \chi(y)(C - k\sigma_{xx}^{\text{total}}(y)). \tag{58}$$

The conditions for single-valuedness of the tangential displacements should also be satisfied. Since the right-hand side in (24) is odd, the solution of (53) is even, i.e., can be presented in the form

$$\varphi(t) = -R(t) \frac{1}{\pi} \int_\Gamma \frac{h(y) y}{R(y)} \frac{dy}{y^2 - t^2}. \tag{59}$$

Therefore in (27) only two independent conditions remain, namely

$$\int_0^L \varphi(t)\, dt = 0, \quad \int_A^B \varphi(t)\, dt = 0. \tag{60}$$

Substitution of (59) in (60) leads to the following system of equations:

$$\begin{aligned} &\int_0^L R(t) \int_0^L \frac{h(y) y}{R(y)} \frac{dy}{y^2 - t^2}\, dt + \int_0^L R(t) \int_A^B \frac{h(y) y}{R(y)} \frac{dy}{y^2 - t^2}\, dt = 0, \\ &\int_A^B R(t) \int_0^L \frac{h(y) y}{R(y)} \frac{dy}{y^2 - t^2}\, dt + \int_A^B R(t) \int_A^B \frac{h(y) y}{R(y)} \frac{dy}{y^2 - t^2}\, dt = 0. \end{aligned} \tag{61}$$

Therefore one has three nonlinear equations (equations (57) and (61)) for the determination of the three unknowns L, A, B. The solution obviously depends on the parameters L_0, C and $k = \tan\rho$. The form of the right-hand side indicates that some solutions may exist; however, the uniqueness is not obvious. The solution of the system has been obtained numerically. Figure 12 shows the results for $L_0 = 0.8$. In particular, it is seen from Figure 12 that the length of the internal shear zone L is rather weakly influenced by the values of cohesion and friction, while the influence of these parameters on the positions of the tips of the external shear zone is much stronger, especially the influence on the position of the external tip of the zone. It is seen that for given values of L_0 and $k = \tan\rho$ the sizes of the external shear zones decrease with increasing cohesion (which is predictable), and at some critical value of cohesion these zones vanish. However, the numerical procedure became extremely unstable for values approaching these critical points.

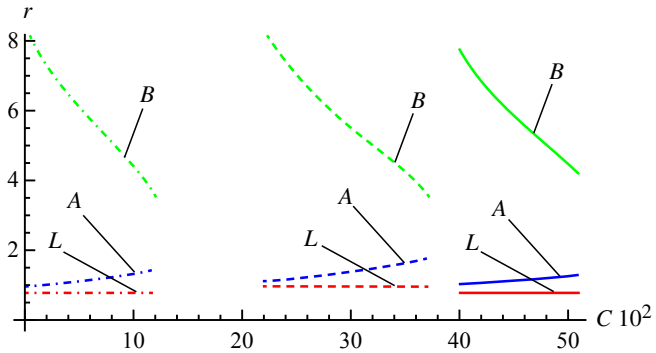

Figure 12. Equilibrium positions of the crack tips depending on relative cohesion C for various k: solid lines correspond to $k = 0$; dashed lines correspond to $k = 0.1$; dash-dotted lines correspond to $k = 0.33$.

7. Conclusion

The problem of wedging of an elastic isotropic homogeneous plane with a weak interface has been solved analytically. The wedge has been modelled by a pair of edge dislocations. The possibility of appearance of either one or three sliding zones (modelled by pure shear cracks) and a delamination zone (combined open-shear crack) along the weak interface has been demonstrated. The positions of the tips of the sliding zones depend on the stresses due to the dislocation, external stress field and the length of the delamination zone, which in turn is determined by the externally applied stress and stresses induced by the dislocation. The positions of the tips of the sliding zones have been computed for a specific configuration.

Acknowledgements

The study was supported by the Russian-Ukrainian Project RFBR-13-01-90430.

References

[Akulich and Zvyagin 2008] A. V. Akulich and A. V. Zvyagin, "Interaction between hydraulic and natural fractures", *Fluid Dyn.* **43**:3 (2008), 428–435.

[Bui 2006] H. D. Bui, *Fracture mechanics: Inverse problems and solutions*, Springer, 2006.

[Bui and Oueslati 2004] H. D. Bui and A. Oueslati, "Solutions exactes de fissure d'interface sous contact frottant avec un milieu indéformable", *C. R. Mécanique* **332**:9 (2004), 709–716.

[Bui and Oueslati 2005] H. D. Bui and A. Oueslati, "The sliding interface crack with friction between elastic and rigid bodies", *J. Mech. Phys. Solids* **53**:6 (2005), 1397–1421.

[Comninou and Dundurs 1983] M. Comninou and J. Dundurs, "Spreading of slip from a region of low friction", *Acta Mech.* **47**:1–2 (1983), 65–71.

[Cook et al. 1964] J. Cook, J. E. Gordon, C. C. Evans, and D. M. Marsh, "A mechanism for the control of crack propagation in all-brittle systems", *Proc. R. Soc. A* **282**:1391 (1964), 508–520.

[Cooke and Underwood 2001] M. L. Cooke and C. A. Underwood, "Fracture termination and step-over at bedding interfaces due to frictional slip and interface opening", *J. Struct. Geol.* **23**:2–3 (2001), 223–238.

[Dundurs and Comninou 1981] J. Dundurs and M. Comninou, "An educational elasticity problem with friction, I: Loading, and unloading for weak friction", *Trans. ASME Ser. E J. Appl. Mech.* **48**:4 (1981), 841–845.

[Gakhov 1966] F. D. Gakhov, *Boundary value problems*, Pergamon Press, New York, 1966. Reprinted Dover, New York, 1990.

[Galybin 1997] A. N. Galybin, "A model of mining-induced fault sliding", *Int. J. Rock Mech. Min.* **34**:3–4 (1997), 91.e1–91.e13. ISRM International Symposium 36th U.S. Rock Mechanics Symposium.

[Galybin and Mukhamediev 2012] A. N. Galybin and S. A. Mukhamediev, "On modelling of fluid-driven fracture branching in jointed rocks", pp. Paper#557 in *19th European conference on fracture, fracture mechanics for durability reliability and safety, Kazan, Russia 26–31, August*, 2012. Published on CD-ROM.

[Galybin and Mukhamediev 2014] A. N. Galybin and S. A. Mukhamediev, "Fracture development on a weak interface ahead of a fluid-driven crack"", *Eng. Fract. Mech.* **129** (2014), 90–101.

[Goldstein and Osipenko 2012] R. V. Goldstein and N. M. Osipenko, "Fracture initiation at the contact under shear", pp. Paper#399 in *19th European conference on fracture, fracture mechanics for durability reliability and safety, Kazan, Russia 26–31, August*, 2012. Published on CD-ROM.

[Goldstein and Osipenko 2015] R. V. Goldstein and N. M. Osipenko, "Initiation of a secondary crack across a frictional interface", *Eng. Fract. Mech.* **140** (2015), 92–105.

[Gorbatikh et al. 2001] L. Gorbatikh, B. Nuller, and M. Kachanov, "Sliding on cracks with non-uniform frictional characteristics", *Int. J. Solids Struct.* **38**:42–43 (2001), 7501–7524.

[Gudmundsson 2011] A. Gudmundsson, "Deflection of dykes into sills at discontinuities and magma-chamber formation", *Tectonophysics* **500**:1–4 (2011), 50–64. Emplacement of magma pulses and growth of magma bodies.

[Mendelsohn and Whang 1988] D. A. Mendelsohn and K. H. Whang, "Partial release and relocking of a frictionally locked crack due to moving tensile loads", *J. Appl. Mech.* (*ASME*) **55**:2 (06/01 1988), 383–388.

[Muskhelishvili 1977] N. I. Muskhelishvili, *Some basic problems of the mathematical theory of elasticity: fundamental equations, plane theory of elasticity, torsion and bending*, English ed., Noordhoff, Leiden, 1977.

[Zhou et al. 2010] J. Zhou, Y. Jin, and M. Chen, "Experimental investigation of hydraulic fracturing in random naturally fractured blocks", *Int. J. Rock Mech. Min.* **47**:7 (2010), 1193–1199.

Received 1 Dec 2014. Revised 19 Jan 2015. Accepted 23 Feb 2015.

ALEXANDER N. GALYBIN: a.n.galybin@gmail.com
The Schmidt Institute of Physics of the Earth, Russian Academy of Sciences, Gruzinskaya str. 10-1, Moscow, 123995, Russia

ROBERT V. GOLDSTEIN: goldst@ipmnet.ru
A. Yu. Ishlinsky Institute for Problems in Mechanics, Russian Academy of Sciences, prosp. Vernadskogo 101-1, Moscow, 119526, Russia

KONSTANTIN B. USTINOV: ustinov@ipmnet.ru
A. Yu. Ishlinsky Institute for Problems in Mechanics, Russian Academy of Sciences, prosp. Vernadskogo 101-1, Moscow, 119526, Russia

JOURNAL OF MECHANICS OF MATERIALS AND STRUCTURES

msp.org/jomms

Founded by Charles R. Steele and Marie-Louise Steele

See msp.org/jomms for submission guidelines.

JoMMS (ISSN 1559-3959) at Mathematical Sciences Publishers, 798 Evans Hall #6840, c/o University of California, Berkeley, CA 94720-3840, is published in 10 issues a year. The subscription price for 2015 is US $565/year for the electronic version, and $725/year (+$60, if shipping outside the US) for print and electronic. Subscriptions, requests for back issues, and changes of address should be sent to MSP.

JoMMS peer-review and production is managed by EditFLOW® from Mathematical Sciences Publishers.

PUBLISHED BY

mathematical sciences publishers

nonprofit scientific publishing

http://msp.org/

Journal of Mechanics of Materials and Structures

Volume 10, No. 3 May 2015

Special issue

In Memoriam: Huy Duong Bui